GEOTECHNICAL INSIGHTS INTO CIRCULAR SHAFT PERFORMANCE IN CLAY

Robert Mair[1] and Njemile Faustin[2]

[1] Emeritus Professor of Civil Engineering and Director of Research
Department of Engineering, University of Cambridge, Cambridge, UK

[2]Senior Geotechnical Engineer
AECOM, UK

ABSTRACT

Shafts are a key aspect of most underground tunnel schemes. Circular shafts are generally preferred over other plan geometries because they are inherently stiffer and more efficient at resisting in-situ horizontal earth pressures. However, there is limited understanding of the performance of these circular shafts and the associated ground movements due to their construction. This paper describes field observations of circular shaft construction assembled from three major tunnelling projects in the United Kingdom and novel centrifuge model tests of shaft excavations in clays that were conducted using the geotechnical centrifuge at the University of Cambridge. Most of the field observations were of settlements adjacent to the shaft; one case study provided novel measurements of longitudinal bending and circumferential hoop strains in a circular shaft lining using innovative fibre optic instrumentation. The wished-in-placed circular shaft in the centrifuge tests was instrumented with strain gauges to measure longitudinal bending and hoop strains. Both the field measurements and the centrifuge tests demonstrated that hoop strains are far more significant than longitudinal bending strains. Miniature displacement transducers installed at varying distances from the shaft measured the adjacent ground surface movements during shaft excavation. Key findings from the field and centrifuge model tests are described.

Notation

α_α - Temperature-induced apparent strain of Brillouin frequency shift

α_b - Thermal expansion coefficient of temperature cable

$\alpha_{concrete}$ - Thermal expansion coefficient of concrete

AL Alluvium

bgl - Below ground level

BOTDR - Brillouin optical time-domain reflectometry

D Diameter

$\Delta\varepsilon_B$ - Differential mechanically induced longitudinal bending strain

$\Delta\varepsilon_H$ - Differential mechanically induced hoop strain

$\Delta\varepsilon_{T,B}$ - Differential combined temperature and mechanically induced longitudinal bending strain

$\Delta\varepsilon_{T,H}$ - Differential combined temperature and mechanically induced hoop strain

$\Delta\varepsilon_T$ - Differential temperature-induced strain

$\Delta\varepsilon_{TR}$ - Differential temperature-induced raw strain

ΔT - differential temperature

i – subscript denoting the internal face of shaft

o - subscript denoting the external face of shaft

H Shaft excavation depth

K_o Lateral earth pressure coefficient (at rest)

LC London Clay Formation

MG Made Ground

OCR over-consolidation ratio

s_u Undrained shear strength

S_v Settlement

RTD River Terrace Deposits

t thickness of the shaft lining

TBM Tunnel boring machine

x Distance from the shaft lining

σ_{hoop} Hoop stress in the shaft lining

σ_h Total in-situ horizontal stress

INTRODUCTION

There is an increasing need to understand the performance of circular shafts as the demand for tunnelling infrastructure rises in urban areas. In many cases, there is little choice but to build shafts near to existing buildings or buried utility services. The potential impact of shaft construction on this existing infrastructure is a concern for engineers. There is also considerable uncertainty surrounding the circumferential compressive stresses in a circular shaft lining (Cabarkapa et al. 2003, Zdravkovic et al. 2005). Monitoring propped rectangular shafts has been widely reported in the literature, but few detailed case studies exist for circular shafts. The uncertainty in shaft design has a direct effect on the cost of circular shaft construction – overly thick shaft linings that may not necessarily be needed are often adopted and protective measures that also may not be needed are sometimes implemented for nearby buildings and services.

Recent construction of three major tunnelling projects in the UK provided a good opportunity to investigate the performance of circular shafts and adjacent ground movements due to their construction. This paper gives some insight into the settlement that occurs adjacent to the shaft and the strains that develop in the shaft lining during excavation. The findings have been obtained from a combination of field observations and centrifuge model testing. Further details of this work are reported by Faustin (2017) and Faustin et al. (2018).

FIELD OBSERVATIONS – SETTLEMENT

The UK's first well-documented circular shaft was constructed for the Heathrow Express. The 11m diameter and 26m deep shaft was constructed primarily through the London Clay Formation using pre-cast segments for the top 16m and a sprayed concrete lining (SCL) for the following 10m. New & Bowers (1994) presented the field measurements of settlement on a plot of settlement normalised by the shaft excavation depth (S_v /H) plotted against the distance, d, from the shaft also normalised by the shaft excavation depth (x/H), as shown in Figure 1. A curve was fitted to the field data which gives a useful empirical correlation to predict settlement due to circular shaft excavation.

It is important to note that this prediction is independent of the shaft diameter and is only suitable for circular shafts constructed in London Clay with a similar geometry and construction method to the Heathrow Express shaft. Consequently, practitioners conservatively use the New & Bowers correlation, together with some engineering judgement to account for different shaft diameters or construction methods. This sometimes leads to significant over-predictions of anticipated settlement.

In recent years, greater insight into the ground response due to circular shaft construction has been obtained from a number of shafts constructed for three major tunnelling projects in the UK: London's new railway, the Elizabeth Line (previously called Crossrail), National Grid's electricity infrastructure upgrade (London Power Tunnels project) and Transport for London's extension of the existing Northern underground tube line. Monitoring data assembled from almost 30 circular shafts constructed for the new tunnels have allowed detailed examination of the settlement arising from circular shaft construction, as described by Faustin et al. (2018). The new case study shafts had a variety of sizes in terms of both diameter and depth. They were all excavated through similar ground conditions comprising varying thicknesses of Superficial Deposits (Made Ground, Langley Silt, Alluvium and River Terrace Deposits) overlying stiff relatively homogeneous London Clay of very low permeability. These strata were underlain by the Lambeth Group, Thanet Sand and Chalk. With the exception of the deeper shaft excavations that extended into or close to underlying permeable strata, there was little groundwater lowering associated with the construction of the case study shafts. Hence settlement due to groundwater lowering is likely to be very small. Details of the decoupling of groundwater-lowering induced movements from the total observed settlements for one deep shaft are reported by Faustin (2017).

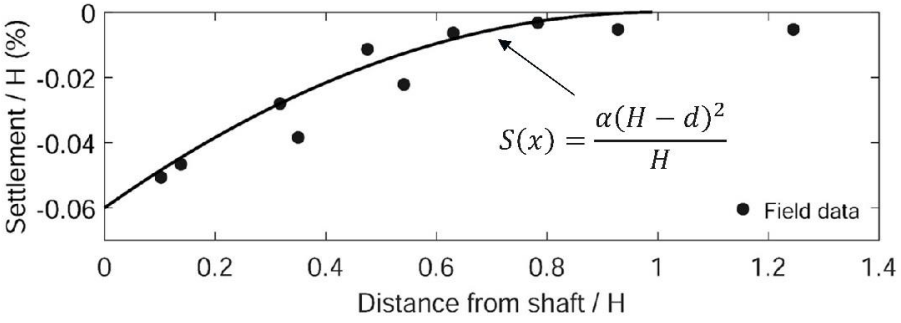

Figure 1 Settlement during excavation of the Heathrow Express shaft in London Basin Deposits (New and Bowers, 1994)

Shaft construction categories

The method of construction for the shafts and its effect on ground movements is important. Two distinct categories of shaft construction were identified: Support Before Excavation (SBE) and Excavation Before Support (EBS).

For the SBE shaft construction category, shown in Figure 2a, the soil is supported by a pre-installed shaft lining before any excavation of the soil within the shaft is undertaken. SBE shaft construction for the case study shafts involved pre-installed diaphragm walls, bored piles or steel sheet piles.

For the EBS shaft construction category, shown in Figure 2b, the soil is first excavated in sections, typically 1.0 m to 1.2 m in height, before the shaft lining support is placed. When a ring is complete, the process is repeated for the underlying ring until the full depth of the shaft is reached. This sequence of erecting the shaft lining after the ground has been exposed is comparable to tunnel excavation ahead of the tunnel lining. As for tunnels, the shaft lining used for the EBS shaft construction category is either pre-cast segments or a sprayed concrete lining (SCL).

Settlement results

Field measurements of settlement for the EBS and SBE shaft construction categories are presented in Figure 3 and 4 respectively. The settlement is presented in a normalised plot of S_v/H versus x/H, where S_v = settlement, x = distance from the edge of the shaft, and H = depth of the excavation within the shaft. Comparison of Figure 3 and 4 shows the influence of the shaft construction category. The local reduction in in-situ total horizontal soil stress and stiffness of the ground when the ground is exposed, prior to placing the support, causes greater settlement around the EBS shaft compared with the SBE construction category. The New & Bowers (1994) correlation, also plotted on Figure 3, is shown to provide a reasonably good estimate of the ground movements for a large number of EBS case study shafts (although less so at distance from the shaft). This is perhaps to be expected since the EBS construction category is applicable to the Heathrow Trial Shaft on which the New & Bowers correlation is based.

The normalised settlement charts, presented in Figure 3 and 4, can be used to make more realistic estimates for shaft design taking account of the different construction methods. Further details of these results are provided by Faustin et al. (2018).

Figure 2 Two distinct shaft construction categories

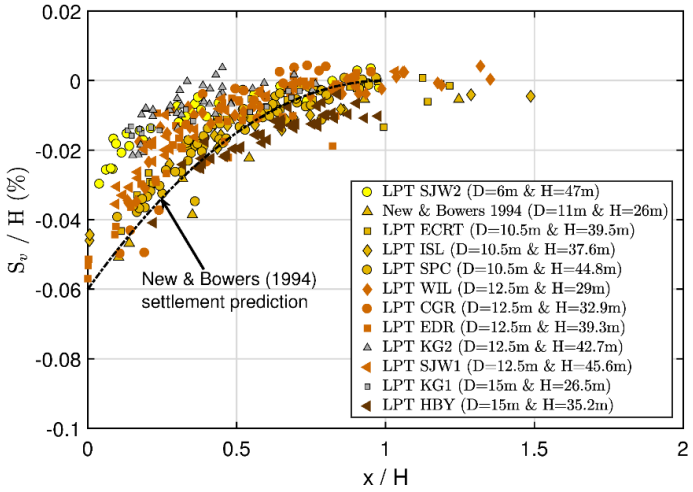

Figure 3 Settlement due to EBS shaft construction (Faustin et al., 2018)

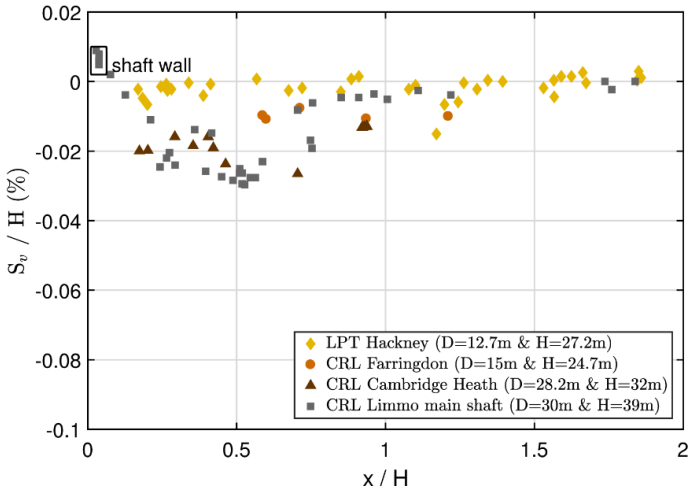

Figure 4 Settlement due to SBE shaft construction (Faustin et al., 2018)

FIBRE OPTIC SENSING PRINCIPLES

Over the last 10 years the Centre for Smart Infrastructure and Construction (CSIC) at the University of Cambridge has explored innovative ways of using fibre optics to measure strains in infrastructure (Kechavarzi et al., 2016). The technology has proven to give accurate and reliable data for improving performance-based design methods, potentially increasing the capacity and efficiency of new infrastructure and construction processes. The fundamental principle of the fibre optic technology is that if a light signal, the incident light, is transmitted through the fibre optic cable then a very small proportion of the light is scattered back to the origin of the signal. It is convenient to view these light signals on a plot of power versus the frequency, as shown in Figure 5. The backscattered light exhibits a peak at some constant value of Brillouin frequency (Figure 5a). When the optical fibres are strained there is a shift in the Brillouin frequency at which this peak amplitude occurs (Figure 5b). By capitalising on the Brillouin frequency shift being proportional to strain, the optical fibre can be used as a continuous strain gauge. A full description of the fibre optic technology and its successful application for civil infrastructure monitoring has been widely reported (e.g. Mohamad, 2008; Soga, 2014; Soga et al., 2015 and Kechavarzi et al., 2016). Two types of fibre optic cables are typically used for these applications:

- a Fujikura reinforced ribbon cable that measures combined mechanical and thermal induced strains.
- an Excel eight-core single mode fibre that measures thermal induced strains (Excel OS1 8C 9/125). Fibres in this temperature cable are surrounded by a liquid gel and therefore not affected by mechanically induced strains.

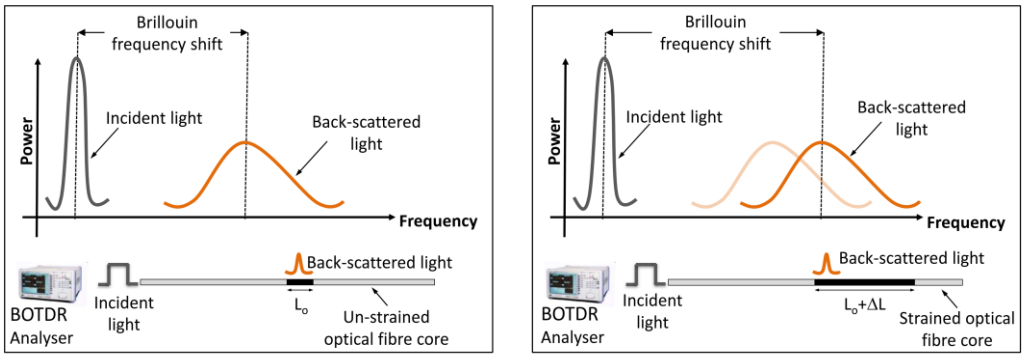

(a) Initial condition: unstrained fibre optic cable **(b)** Strained fibre optic cable

Figure 5 Principles of fibre optic sensing technology

FIELD OBSERVATIONS – FIBRE OPTIC STRAINS

Fibre optic sensors were used to monitor strains in the main tunnel boring machine (TBM) launch shaft in east London for the UK's new railway, the Elizabeth Line (previously called Crossrail). The work was carried out under a collaborative Knowledge Transfer Partnership between the University of Cambridge and Crossrail Ltd. The 30m diameter case study shaft falls under the SBE construction category, being supported by fourteen 1.2m thick, 53m long diaphragm wall panels. Five pairs of 1.1 m thick and 10 m long prefabricated steel reinforcement cages, installed in each diaphragm wall panel, were lowered into the excavated slurry-filled diaphragm wall trench. The shaft was then excavated to a maximum depth of 45m through typical London Basin strata, as illustrated in Figure 6.

Three diaphragm wall panels of the shaft were instrumented with fibre optic cables (Figure 7). Three different fibre optic cables were secured to the reinforcement cage in each diaphragm wall panel. The Fujikura reinforced ribbon cable was secured longitudinally and radially to monitor longitudinal bending strains and hoop strains respectively, as shown in Figure 8. The internal face of the diaphragm wall panels was progressively exposed during excavation of the shaft while the bottom part remained embedded in the ground. To separate the thermal-induced strains (from curing concrete) from the mechanically induced strain due to excavation, a temperature cable was installed longitudinally alongside the Fujikura reinforced ribbon cable.

The instrumentation procedure developed for the fibre optic sensors caused minimal disruption to the diaphragm wall panel construction (Figure 8). As the reinforcement cages were lowered the fibre optic cable was uncoiled from a cable drum and fixed to the cages at intervals. Steel brackets were welded to the reinforcement cages while they were stored on site and the Fujikura reinforced ribbon cable was attached via a bespoke clamp which was designed to connect to the brackets (Figure 9). Adjustment of the nuts on either end of the clamps allowed a pre-tension of approximately 1500 to 2000 microstrain (1500 to 2000 με) to be applied to the Fujikura reinforced ribbon cable. The optical fibre cable to monitor temperature was loosely fixed using cable ties. Figure 9 shows a photo of a typical instrumented reinforcement cage and Figure 10 shows the lowering of an instrumented reinforcement cage into an excavated diaphragm wall panel.

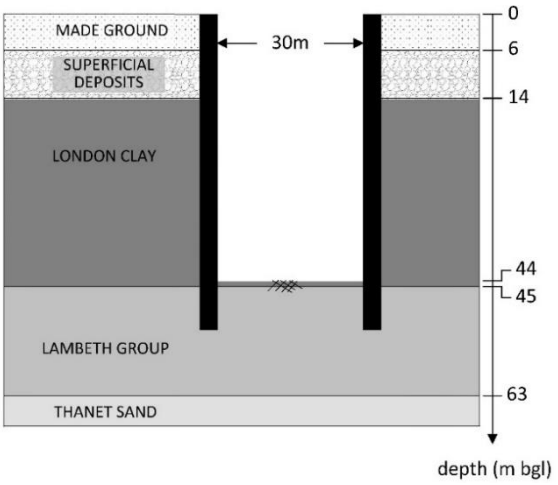

Figure 6 Schematic profile of the instrumented SBE shaft

Ideally, an initial baseline reading should be taken after the diaphragm wall panel was constructed i.e. a reference reading. However, due to heavy equipment and plant congestion on the site, the fibre optic monitoring system was commissioned when the shaft excavation depth was already 13.5 m below ground level (bgl). Subsequent measurements were taken at 3 m excavation intervals. Measurements comprised a minimum of three readings from each fibre optic cable and an average of the three readings are presented relative to an excavation depth of 13.5 m bgl.. These readings were taken using a Brillouin optical time domain reflectometry analyser manufactured by Yokogawa (AQ8603 BOTDR). This analyser used the spontaneous Brillouin scattering of the light signal to provide strain values every 5 cm at a resolution of 30 microstrain (30 με) with a spatial resolution of 1.0 m (Yokogawa, 2005).

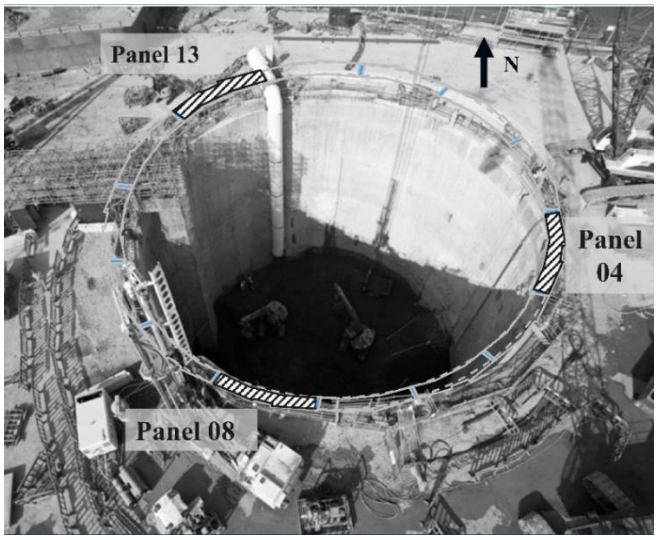

Figure 7 Aerial view of SBE shaft showing the instrumented diaphragm wall panels

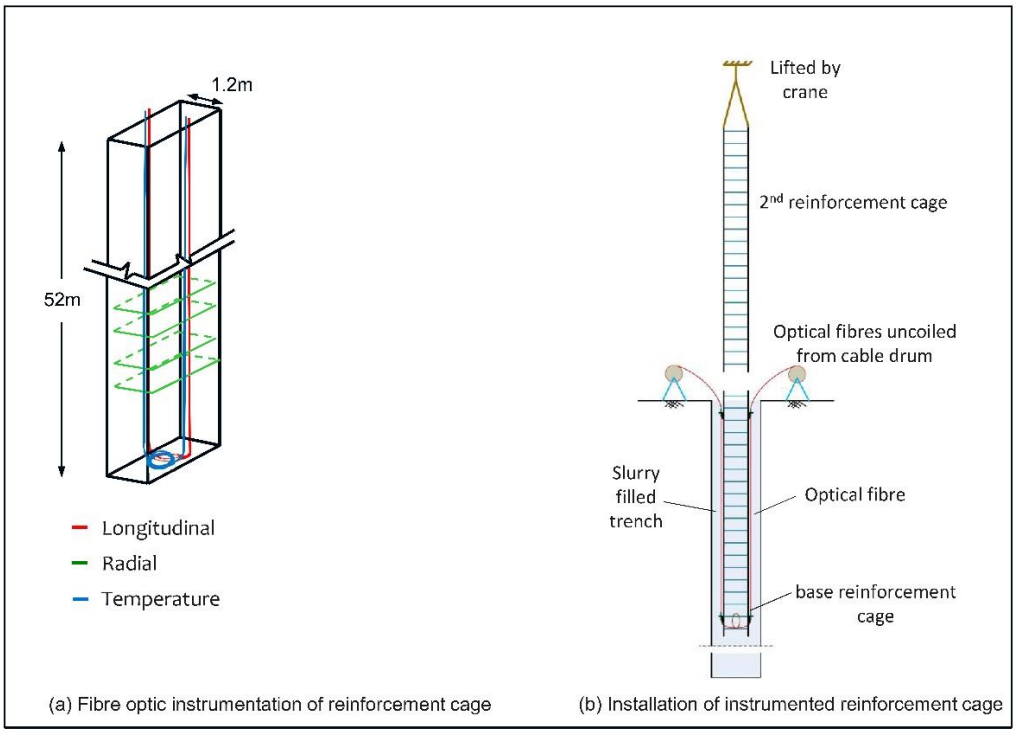

Figure 8 Schematic of a typical fibre optic installation

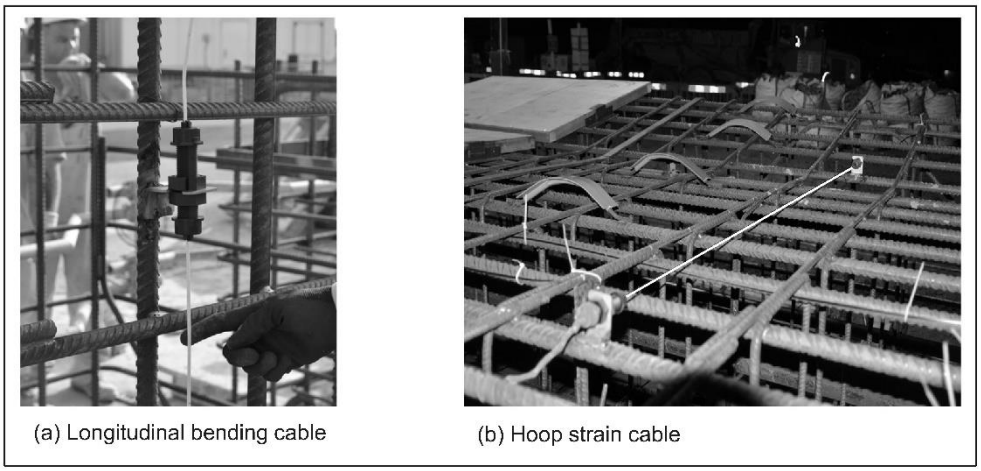

Figure 9 Attachment of fibre optic cables to reinforcement cage

Figure 10 Installation of fibre optic instrumented reinforcement cage

Fibre optic strain measurements

Compensation for temperature effects was carried out using Equation (1) to obtain the differential mechanically induced longitudinal bending ($\Delta\varepsilon_B$) or circumferential hoop strain ($\Delta\varepsilon_H$) due to excavation of the shaft only.

$$\Delta\varepsilon_B = \Delta\varepsilon_{T,B} - \Delta\varepsilon_T \quad (1)$$

$$\Delta\varepsilon_H = \Delta\varepsilon_{T,H} - \Delta\varepsilon_H \quad (2)$$

where $\Delta\varepsilon_{T,B}$ and $\Delta\varepsilon_{T,H}$ are the differential combined temperature and mechanically induced strain, measured by the Fujikura reinforced ribbon longitudinal and hoop cable respectively and $\Delta\varepsilon_T$ is the differential temperature-induced strain. The $\Delta\varepsilon_T$ parameter was derived from the differential temperature-induced raw strain measured by the temperature cable ($\Delta\varepsilon_{TR}$) using Equations (3) and (4):

$$\Delta\varepsilon_T = (\alpha_{concrete} + \alpha_\alpha)\Delta T \quad (3)$$

where $\alpha_{concrete}$ is the thermal expansion of the concrete (10 με/°C), α_α is the temperature-induced apparent strain of Brillouin frequency shift (19.47 με/°C) and ΔT is the temperature change at either side of the diaphragm wall, calculated using Equation (3)

$$\Delta T = \Delta\varepsilon_{TR}/(\alpha_b + \alpha_\alpha) \quad (4)$$

where $\Delta\varepsilon_{TR}$ is the differential temperature-induced raw strain measured from temperature cable and α_b is the thermal expansion coefficient of the temperature cable (4.2 με/°C). Further details of this temperature compensation are reported by Mohamad (2008).

Longitudinal bending strains

Longitudinal bending strains observed in the three panels were similar and typical measurements for Panel 4 at two excavation depths, 18.9 m and 33.5 m, are presented in Figure 11. The combined temperature and mechanically induced strain ($\Delta\varepsilon_{T,B}$) and the temperature-induced strain ($\Delta\varepsilon_T$) measurements are shown relative to the initial reference reading for both the internal and external face of the shaft. The combined temperature and mechanically induced strain is seen to be marginally greater than the strain due to temperature changes only. This indicates that most of the strain arises from temperature changes when the internal face of the shaft is exposed during excavation and there is little strain due to mechanical effects i.e. displacement of the shaft lining during shaft excavation.

The fibre optic measurements showed that the change in temperature due to excavation is different along the diaphragm wall panel. Temperature-induced strains were approximately 200 microstrain greater on the internal face of shaft ($\Delta\varepsilon_{T_i}$) which is exposed during excavation compared with the external face of the shaft ($\Delta\varepsilon_{T_o}$). This corresponds to a temperature difference of approximately 8.5 degrees Celsius, based on Equation (4). Below the excavation level, the strains are similar on both the internal and external face of the shaft lining.

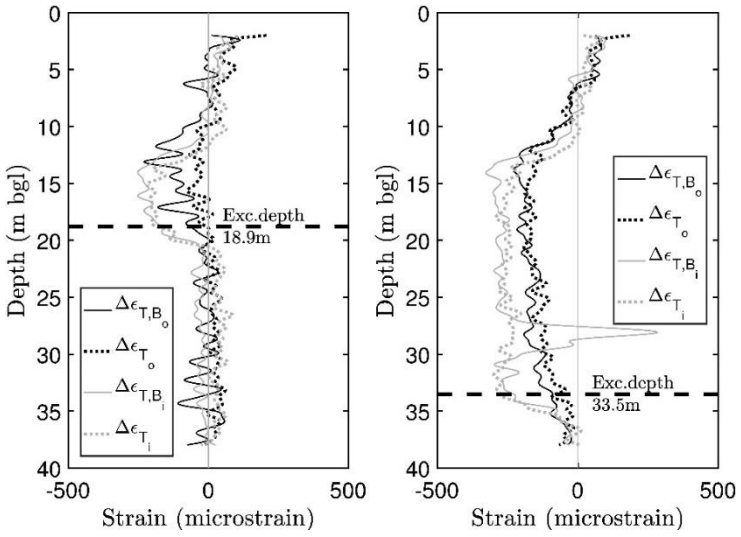

Figure 11 Measured longitudinal bending strains in Panel 4 during excavation

Hoop strains

Figure 12 shows the development of circumferential hoop strain in one of the diaphragm wall panels during excavation of the case study shaft. The strain measurements represent the response of the fibre optic cables positioned at a depth between 28.8 m and 32.52 m bgl. The elevation of the hoop strain cables is shown as a grey shaded area on Figure 12 and the symbols represent hoop strain measurements at the installed fibre optic cable depth for different excavation levels. Negative strain values represent circumferential compression of the circular shaft lining and positive values indicate tension.

Initially, the increase in hoop strain was relatively small, but the strains increased when the excavation level proceeded beyond the hoop cable level. At the end of shaft excavation, the hoop strain was approximately 400 με. This corresponds to a maximum radial movement of the diaphragm wall panels of approximately 6 mm using a mean radius of 15.6 m for the shaft.

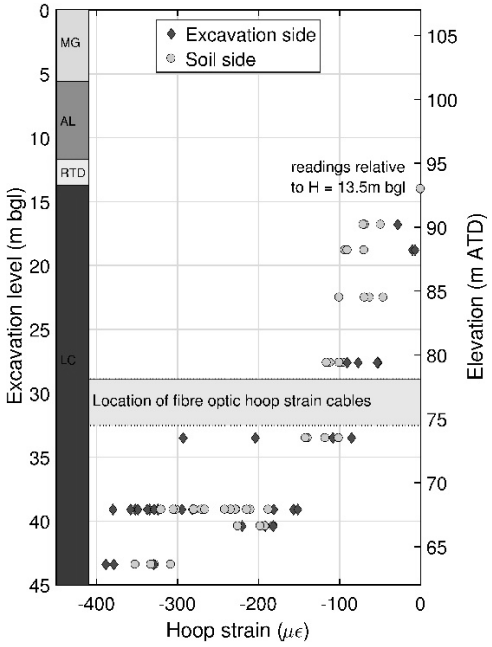

Figure 12 Fibre optic hoop strain measurements during excavation

CENTRIFUGE TESTING

The final part of this paper describes some centrifuge model tests that were carried out using the 10 m diameter geotechnical centrifuge at Cambridge University. A detailed description of this centrifuge is given by Schofield (1980). Typically, excavations are carried out by replacing the soil to be excavated with a heavy fluid that is then drained during the centrifuge test. This creates a condition in which horizontal and vertical soil stress changes are equal, which may not actually be the case in practice. The development of strains in the shaft lining is dependent on the soil stress changes during excavation. Therefore, to allow these strains to be more accurately examined, a novel auger excavator was designed and built to remove clay in-flight from inside the shaft.

Figure 13 shows the centrifuge package and a typical cross section through the centrifuge model. The 100 mm diameter and 1mm thick aluminium shaft was embedded in over-consolidated clay before the centrifuge test i.e. the SBE shaft construction category. The centrifuge package was then placed in the centrifuge where a staged excavation of the shaft to 140 mm was carried out under a centrifugal acceleration of 75g. At prototype scale, this is equivalent to a 7.5 m diameter shaft excavated to 10.5 m depth.

The centrifuge model was well instrumented. A series of pore pressure transducers were embedded in the clay to monitor the stress history of the clay during preparation of the centrifuge model and during the centrifuge test. Strain gauges configured in Wheatstone full bridge and half bridge circuits were secured to the model shaft, before it was embedded into the clay, to monitor bending and hoop strains in the shaft lining. A series of miniature displacement transducers were also positioned on the clay surface at varying distances from the shaft to monitor displacement of the surrounding ground during the centrifuge tests. The centrifuge apparatus is described below. Further details are provided by Faustin (2017).

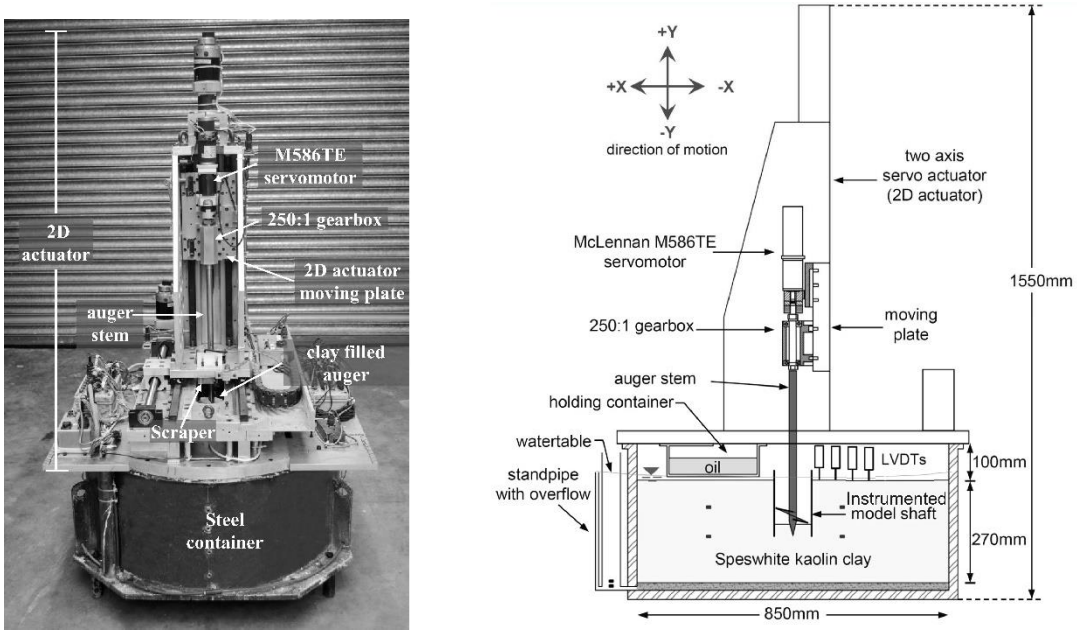

Figure 13 Centrifuge model apparatus

Material properties - Speswhite kaolin clay

Preparation of the clay model was an important part of the centrifuge test. First, a slurry consisting of Speswhite kaolin clay powder and water was mixed to about 1.2 times its liquid limit, equivalent to a moisture content of 125 %. The slurry was consolidated at 1g to a maximum vertical effective stress of 400 kPa, before being allowed to swell over a period of many hours to a linearly increasing vertical stress of up to 140 kPa in the centrifuge test. The undrained shear strength of the clay derived using a relationship proposed by Vardanega et al. (2012), increased with depth to a maximum of approximately 50 kPa at the base of the clay model. Figure 14 shows the inferred undrained shear strength (s_u) profile, over-consolidation ratio (OCR) and K_o profile of the clay. The latter is based on the well-known empirical relationship reported by Schmidt (1983).

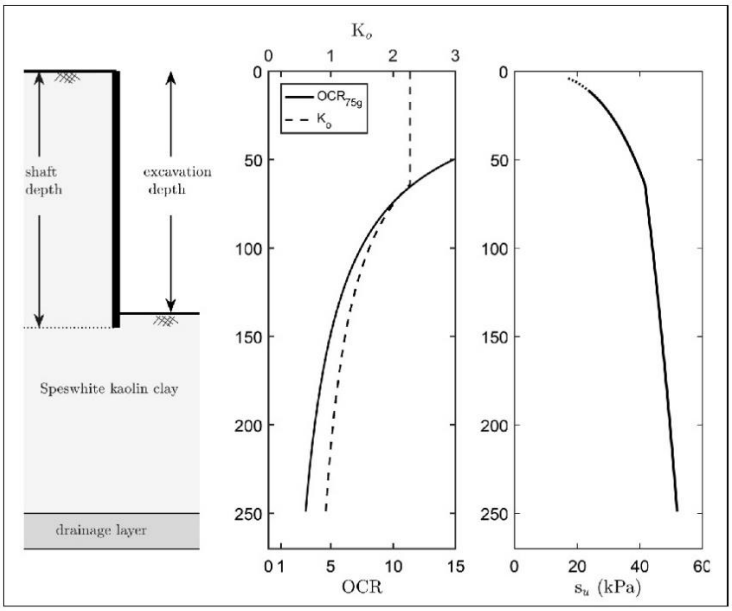

Figure 14 Material properties of the Speswhite kaolin clay at 75g.

Main apparatus

The miniature auger excavator, developed to excavate the model shaft in-flight, comprised a single flight auger to excavate clay from the centre of the shaft, a two axis servo-actuator (2D actuator) to control movement of the auger in the horizontal and vertical direction and a mechanical device to remove the excavated clay from the auger after each excavation step. The model container with the 2D actuator connected on top are shown in Figure 13.

The auger had an outer diameter of 88 mm which was specially designed to allow a 6 mm clearance between the auger and the inner wall of the shaft lining. The stem of the auger, connected to the output shaft of a McLennan IP57-M03 250:1 gearbox, was mounted onto the moving plate of the 2D actuator. This allowed the auger to be moved in both the horizontal and vertical direction. A connection to a M586TE servomotor allowed the auger to rotate.

The 2D actuator was programmed to lower the rotating auger into the clay to excavate approximately 100 mm of clay. After each excavation interval, the auger with the excavated clay on its blade, was raised out of the shaft and transported horizontally across the model container to a holding container (Figure 13). In this position, the excavated clay was removed from the auger using a 35 mm square aluminium block (scraper) mounted above the auger (Figure 13). The scraper was connected to an electro-mechanical linear actuator that allowed it to move downwards, connect with the rotating auger and clean the clay off it. Once this was complete, the auger returned to its central position above the shaft ready to perform the next excavation step.

Typical centrifuge test results

As expected for a small SBE shaft that is supported by a shaft lining before the excavation is carried out, very small displacements were recorded around the model shaft during excavation. Settlement of the clay only became dominant when basal failure was approached (Faustin 2017). As a result, the findings presented in this paper will focus on the circumferential or hoop strains measured in the shaft lining during excavation. Similar to the fibre optic field measurements, the centrifuge results of longitudinal bending strains were considerably smaller than the hoop strains.

Figure 15 shows the typical development of hoop stresses observed in the shaft lining as the excavation progressed. The results were derived from hoop strains recorded by a strain gauge positioned at a depth of 55 mm bgl. Positive stresses indicate tensile hoop stresses and negative values compressive hoop stresses. Similar to the fibre optic field observations, the hoop stresses are observed to increase as the excavation progresses. At the end of excavation, the compressive hoop stress in the shaft lining at 55 mm bgl, derived from strain measurements is 3.9 MPa. Considering a typical cross section through the shaft during excavation (Figure 16), the derived compressive hoop stress can be compared to a prediction of hoop stress calculated using simple cylindrical shell theory:

$$\sigma_{hoop} = {}^{\sigma_h D}/_{2t} \qquad (5)$$

where σ_{hoop} is the hoop stress in the shaft lining, σ_h is the total in-situ horizontal stress acting on the model shaft lining, D is the diameter of the model shaft and t is the thickness of the shaft lining. Equation 5 assumes that the soil imparts a uniform horizontal stress on the model shaft lining and that there is negligible inward movement of the shaft lining during excavation. Assuming an average K_o of 1.5 (see Figure 14), Equation 5 indicates that the total in-situ horizontal stress acting on the shaft is expected to generate a hoop stress of 4.2 MPa in the shaft lining when the excavation depth is at 55 mm bgl. The prediction is slightly higher than the hoop stresses derived from the strain measurements, as the shaft lining can be expected to experience a small reduction in diameter due to excavation of the shaft. This would cause the total in-situ horizontal stress acting on the shaft to be lower than estimated from the K_o 'at rest' condition.

Figure 15 also shows the results of an axisymmetric finite element analysis of the centrifuge excavation using PLAXIS 2D. The undrained total stress analysis was based on identical geometry and material parameters as the centrifuge model and a Mohr Coloumb constitutive model in which the strength of the clay was defined using the undrained shear strength profile shown in Figure 14 (cohesion = s_u) with zero friction angle and zero dilatancy angle. The experimental data for the deeper excavation depths are bounded by the simple cylindrical shell theory and the finite element results.

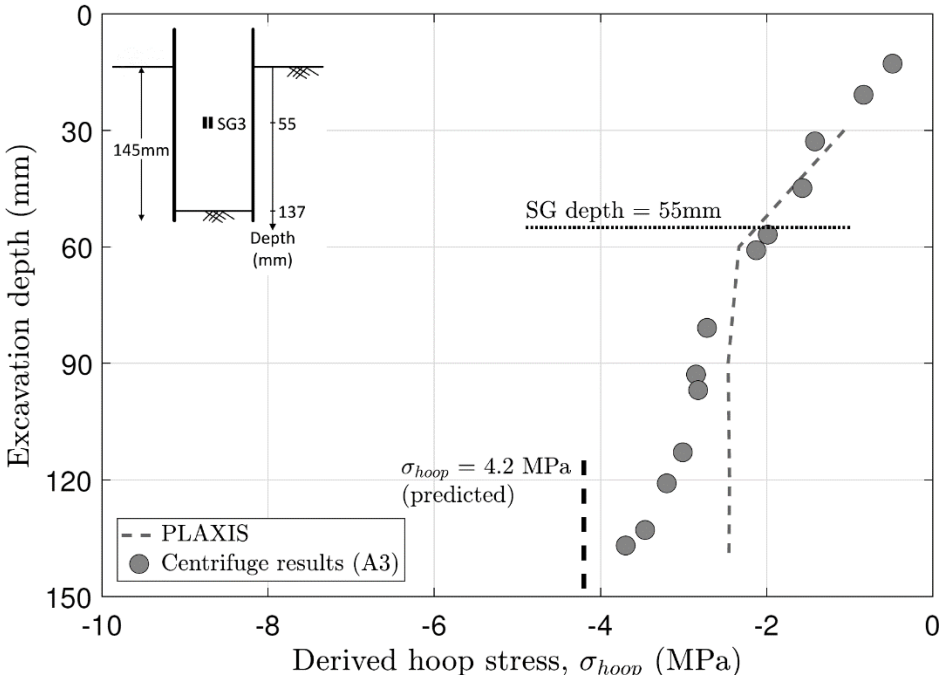

Figure 15 Derived hoop stress from strain readings

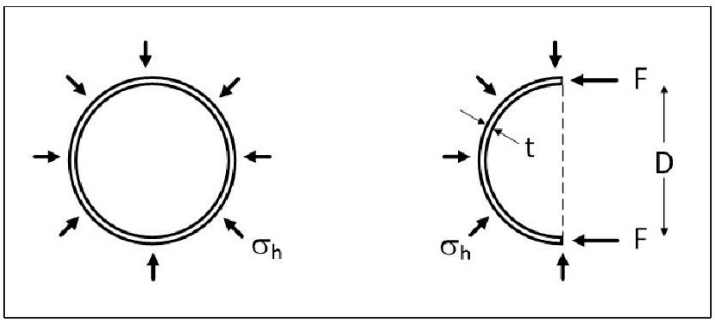

Figure 16 Schematic of stresses at a given elevation of the shaft

CONCLUSIONS

The combination of field observations and centrifuge test results presented in this paper provide new insights into the strains induced in circular shaft linings and settlement of the adjacent ground during their construction. The findings are useful for future design of shafts in clays. Before now few detailed case studies existed for circular shafts, which made it difficult to calibrate analyses predicting their performance and to reliably estimate the magnitude and extent of adjacent ground movement.

The category of shaft construction has been demonstrated to influence how the adjacent ground is impacted by the shaft construction. Two different shaft construction categories are identified: Support Before Excavation (SBE) and Excavation Before Support (EBS). For the SBE shaft construction category, the shaft lining is installed before excavation is carried out whereas for the EBS shaft construction category, the soil is excavated first before the support or shaft lining is placed. Importantly, smaller settlements were measured in the case of the SBE shafts. Field measurements of settlement presented for shafts of different diameters and depths, constructed in London, allows accurate empirical predictions of the settlement due to circular shaft excavation, taking account of these different shaft construction categories and different geometries.

Fibre optic sensors embedded in the diaphragm walls of the Elizabeth Line TBM launch shaft provided valuable insight into the strains developing in a circular shaft lining during excavation. The field strain measurements corroborated well with the centrifuge test results. In both cases, longitudinal bending strains were very small in comparison to the circumferential hoop strains, which develop to resist in-situ horizontal soil stresses. Simple cylindrical shell theory was

shown to provide a good approximation of the maximum hoop stresses in a circular shaft. This may prove useful for designers before more advanced finite element analyses are carried out.

ACKNOWLEDGEMENTS

The authors are grateful to the Engineering and Physical Sciences Research Council (Award Reference 1220514) and Geotechnical Consulting Group for financial support. Special thanks are given to Dr Mohammed Elshafie and Mr. Neil Houghton for their contribution to the design of the new apparatus and to Mr Clive Dalton and Cambridge Insitu Limited for the strain gauging. The invaluable contribution from the technicians at the Schofield Centre at Cambridge University is gratefully acknowledged.

REFERENCES

Cabarkapa Z et al. (2003). *Design and performance of a large diameter shaft in Dublin boulder Clay*. In Proceedings of Foundations: Innovations, Observations, Design and Practice (Newson TA (ed.)), 10.1680/fiodap.32446.0017.

Faustin, NE. (2017). *Performance of Circular Shafts and Ground Behaviour during Construction*. PhD thesis, University of Cambridge, Cambridge, UK.

Faustin, NE, Elshafie, MZEB and Mair, RJ. (2018). *Case studies of circular shaft construction in London*. Proceedings of the Institution of Civil Engineers - Geotechnical Engineering 171(5), 391 – 404. https://doi.org/10.1680/jgeen.17.00166

Kechavarzi C et al. (2016). *Distributed fibre optic strain sensing for monitoring civil infrastructure: A practical guide*. ICE Publishing, London, UK, 10.1680/dfossmci.60555.bm.

Mohamad H. (2008). *Distributed Optical Fibre Strain Sensing of Geotechnical Structures*. PhD thesis, Cambridge University, Cambridge, UK.

New, B. and Bowers, K. (1994). *Ground movement model validation at the Heathrow Express trial tunnel*. In Tunnelling ’94 Proc. 7th Int. Symp. IMM and BTS, pages 301–329, London. Chapman and Hall.

Schmidt, B. (1983). *Discussion: Ko-OCR relationships in soil*. J. Geotech. Eng., ASCE 109(6), 866–867.

Schofield, A. N. (1980). *Cambridge geotechnical centrifuge operations*. Géotechnique,30(3):227–268.

Soga K. (2014). XII Croce Lecture: *Understanding the real performance of geotechnical structures using an innovative fibre optic distributed strain measurement technology*, Rivista Italiana di Geotecnica, vol 4, pp. 7-48.

Soga K et al. (2015). *The role of distributed sensing in understanding the engineering performance of geotechnical structures*. Proceedings of the XVI European Conference on Soil Mechanics and Geotechnical Engineering, Edinburgh, 10.1680/ecsmge.60678.vol1.002.

Vardanega, P et al. (2012). *Laboratory measurement of strength mobilisation in kaolin: link to stress history*. Géotechnique Letters, 2(1): 9–15.

Yokogawa. (2005). *AQ8603 Optical Fiber Strain Analyzer*. Website: http://cdn.tmi.yokogawa.com/files/uploaded/buaq8603_00e_1.pdf (Date Accessed 10/01/2019).

Zdravkovic L et al. (2005). *Modelling of a 3D excavation in finite element analysis*. Géotechnique, 55(7): 497–513, https://doi.org/10.1680/geot.2005.55.7.497.